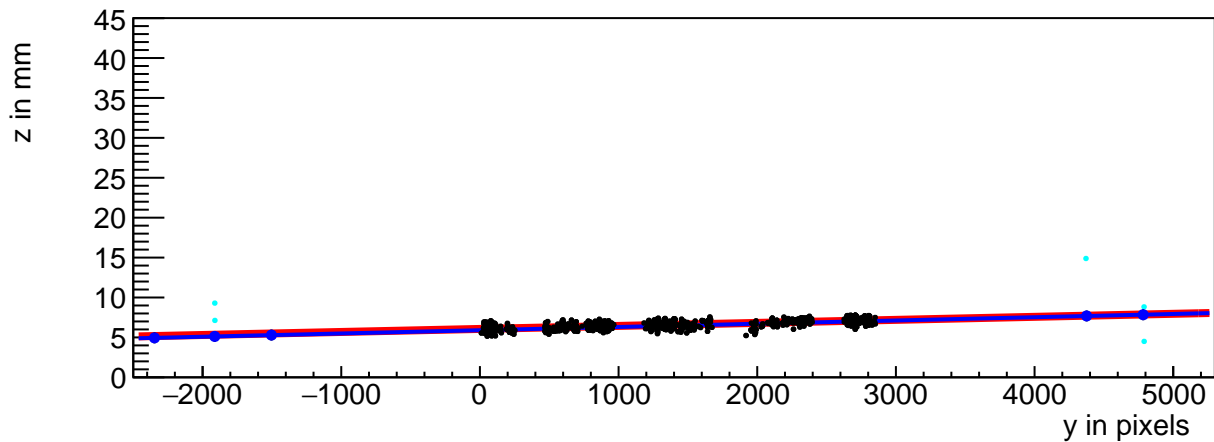
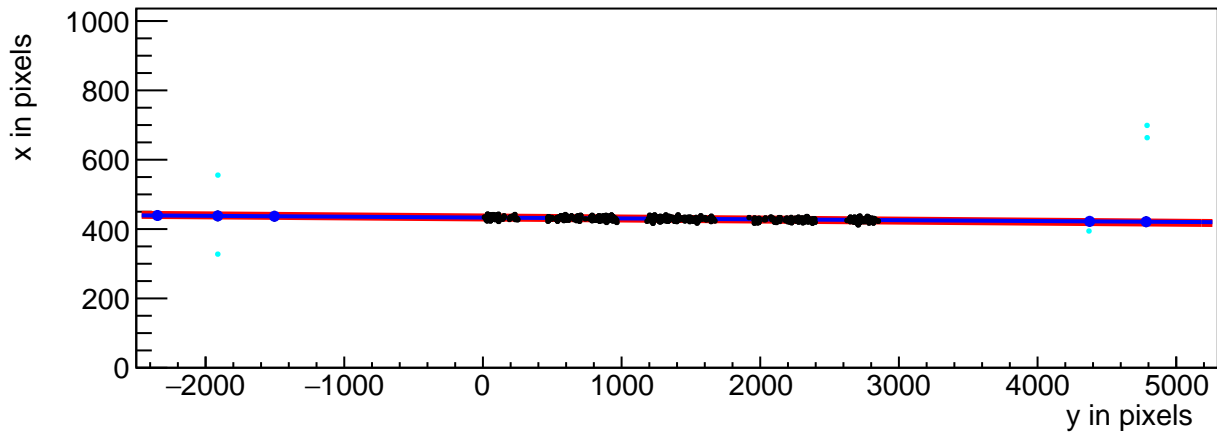


Nuclear Inst. and Methods in Physics Research, A

Towards a Pixel TPC part I: construction and test of a 32-chip GridPix detector

--Manuscript Draft--

Manuscript Number:	NIMA-D-24-00682R2
Article Type:	Full length article
Section/Category:	High Energy and Nuclear Physics Detectors
Keywords:	Micromegas, gaseous pixel detector, micro-pattern gaseous detector, Timepix, GridPix, pixel time projection chamber
Corresponding Author:	Peter Kluit, Ph.D. Nationaal Instituut voor subatomaire fysica Amsterdam, Noord-Holland NETHERLANDS
First Author:	Peter Kluit, Ph.D.
Order of Authors:	Peter Kluit, Ph.D. Jochen Kaminsky, Dr other authors not listed here
Abstract:	<p>A Time Projection Chamber (TPC) module with 32 GridPix chips was constructed and the performance was measured using data taken in a testbeam at DESY in 2021. The GridPix chips each consist of a Timepix3 ASIC (TPX3) with an integrated amplification grid and have a high efficiency of about 85% to detect single ionisation electrons.</p> <p>In the testbeam setup, the module was placed in between two sets of Mimosas26 silicon detector planes that provided external high precision tracking and the whole detector setup was slid into the PCMAG magnet at DESY.</p> <p>The TPC could be operated reliably and used a 93.6/5.0/1.4 gas mixture (by volume) of Ar/iC4H10/CO2 with a small amount of oxygen and water vapour.</p> <p>The analysed data were taken at electron beam momenta of 5 and 6 GeV/c and at magnetic fields of 0 and 1 Tesla(T).</p> <p>The result for the transverse diffusion coefficient DT is $(287.2 \pm 0.5) \mu\text{m}/\sqrt{L}$ at $B = 0$ T and DT is $(120.3 \pm 0.5) \mu\text{m}/\sqrt{L}$ at $B = 1$ T.</p> <p>The longitudinal diffusion coefficient DL is measured to be $(251 \pm 14) \mu\text{m}/\sqrt{L}$ at $B = 0$ T and $(224 \pm 14) \mu\text{m}/\sqrt{L}$ at $B = 1$ T.</p> <p>Results for the tracking systematical uncertainties in xy (pixel plane) were measured to be smaller than $13 \mu\text{m}$ with and without magnetic field.</p> <p>The tracking systematical uncertainties in z (drift direction) were smaller than $15 \mu\text{m}$ ($B = 0$ T) and $20 \mu\text{m}$ ($B = 1$ T).</p>
Opposed Reviewers:	



Dear Reviewers

A very happy new year to you and your family.

Thank you for the very careful reading of the manuscript. Your comments and questions have improved the quality of the manuscript significantly.

Here below the replies/[answers](#) to questions and remarks and [actions](#) in blue that were taken.

See you Peter Kluit

Reviewer #1: Dear authors, thank you for addressing in detail point by point comments and for improving the manuscript.

Reviewer #2: The first revision of the manuscript has been improved on many points of criticism mentioned in the review. However, there are still some items that should be considered before publication. Some of the points below are actually a repetition of previous comments, which were not addressed, despite the authors claim in their response that they were taken into account. It is needless to say that it is quite tiring having to cross-check and repeat these. Some typos or semantic problems could have been spotted by careful proofreading of the full paper before resubmitting it.

Section 5:

The definition of the residual in line 214f is still not satisfactory. Being a distance, it cannot be the "closest point" as stated here. The authors should be more careful, taking into account that this was already brought up in the first review. Since I want to avoid more iterations on this, I suggest the following (if I have understood the authors' intention correctly):

"The track residual in xy is defined as the closest distance between the hit at

the center of the pixel and the xy-projection of the track. The residual in z is calculated at this point of closest approach on the track."

However, this definition of the residuals (which is not standard in my opinion) brings up the following question:

-> Apparently there is still some misunderstanding of the meaning of the words and precise definition of the distance and residual.

Section 4.2:

The authors should mention in line 188, which quantity is actually minimized in the track fit. Normally, one would expect that the track fit minimizes the squared 3-D distances from the hits to the track, weighted by the respective uncertainties in xy and z. If this is indeed what has been done, why then are the residuals in Sec. 5 defined as the closest distance of approach in the xy plane? Unless the uncertainties on z are much larger than the ones in xy (which is not the case here), the two quantities are not expected to be the same. Depending on the quantity actually minimized in the fit, it would be more consistent to define the xy residuals as the xy component of the 3D residual, and not the DCA in xy.

Reply: it is only the xy component of the 3D distance that is minimized (excluding the z component).

Text was: "The track residual in xy is the closest point of the hit at the center of the pixel to track in the xy plane"

Proposal is: "The track residual in xy is defined as the closest distance - defined as the 2D xy projection of the 3D distance between the hit at the center of the pixel and the track."

Section 5.3, lines 303-322 and 344-357:

The authors did not really attempt to improve this part. The procedure of regrouping and superimposing chips is still not clear. Changing "four 256x256" to "(4x256)x256" does not change anything. The example is not very helpful

either. The authors should explain clearly and unambiguously, HOW they are regrouping and combining chips, and, most of all, WHY they are doing it in this particular way. E.g. investigating deformations along the x or y-axis, etc.

Reply: We did give an intuitive/descriptive picture of the procedure. We understand that for clarity it is useful to give the mathematical procedure and add this as a footnote.

New text:

“In order to reduce the statistical fluctuations and quantify the tracking precision, the pixels were regrouped into larger bins respecting the module geometry. After the regrouping procedure, a module plane with $(4 \times 256) \times 256$ bins is obtained, as shown in Figure \ref{fig:deformationsGroupedB0} \footnote[1]{The mathematical procedure is defined as follows. The original mean residual - before rebinning - is given by $\text{residual}(i,j)$ where i runs horizontally and j vertically. The rebinned result for the residual $(4 \times 256, 256)$ is equal to $\text{residual}(i \times 1024, j \times 256)$. The mean residual $(256, 4 \times 256)$ - discussed later in the paper - is equal to $\text{residual}(i \times 256, j)$.”

Section 5.4:

The term tracking precision is still not defined. Is it the average track uncertainty propagated to the plane at $y=1436$? As requested in the first review, the authors should also give the standard deviation of these numbers to quantify the width of the distribution.

Reply: The text reads:

" The tracking precision in the middle of the TPC (at $y = 1436$ pixels) was derived on a track-by-track basis, by propagating the pixel TPC hit uncertainties."

So yes: the "track uncertainty propagated to the plane at $y=1436$ "

Second point: Indeed, in the reply we should have mentioned the standard deviation on the uncertainties. The rms on the uncertainties in xy is 2.4 microns and in z 2.8 microns.

Section 6:

Ref. [4] is not publicly accessible. Why not show the ToT distributions here, as suggested in the first review? Especially since quantitative results are quoted and discussed for ToT.

Reply: Ref [4] is a publicly available result. In Figure 6 of ref [1] the ToT distribution is also shown. Proposal: in the text we also cite the published plot in ref [1].

We also fixed the embedded https link in the reference.

The term "deposited charge" is misleading. Deposited in the detector or in the pixel? It probably should be the "charge after avalanche multiplication,

Reply: Yes that is clearer.

Old text "The time over threshold is related to the deposited charge."

New: "The time over threshold is related to the charge after avalanche multiplication" collected by a given pixel". In line 386, it should probably read "the mean collected charge per pixel", contrasting it with "the most probably value" in the next line.

Reply: Yes that is better

Old text "This means that the deposited charge per pixel .."

-> "This means that the mean deposited charge per pixel .."

The reasoning in line 391ff is difficult to follow: For B=0T, the mean number of e-ion pairs predicted by MagBoltz is 106. The mean number of hits is measured to be 124. Should these two numbers be directly compared for the agreement?

Reply: One could compare the mean and mop values of the B=0 and 1 T data to the Magboltz expectation, taking into account that in the observed mean number of hits there is also a contribution from hits produced by photons in the avalanche process. That process is not included in the Magboltz expectation(s).

Minor comments from the reviewer:

- references: use [1,2], not [1], [2].

Done

- check hyphenation, especially for compounds, e.g. "high-precision tracking", "single-electron resolution", "follow-up paper"

Done

- line 53: "envelope"

Done

- line 108: semi colon or full stop before "this"

Done

- Figure 2 caption, line 5: "as"

Done

- Tables 1 and 2 are still not formatted properly

Done added top and bottom rules (lines)

- line 163: check language "were selected were required"

Done

- line 183: add "...wide in z, corresponding to the size of the quartz window, were not...."

Done

- line 191: "at"

Done

- line 204f: This sentence is not clear: What are the items in parentheses?

"Row" and "column" are not defined. Why not use dx/dy , ... instead?

Done. The parentheses give the different coordinates and angles. A proposed by the reviewee, now x and y are used instead of row/columns

- Figure 4: In the upper plot, the black dots for $0 < y < 3000$ seem to be covered by blue symbols. Please check! Why are there only two and not three Mimosa hits for $y > 4000$?

Done. The plot is remade with the right color coding.

Answer: The detector/clusterisation is not 100% efficient and one (2D) hit is lost.

- Figure 4 caption: "(top) in the precision plane (x,y) and (bottom) drift plane (z_drift,y)".

Done

- line 219/221: As I understand, the arguments under "Firstly" and "secondly" are not 2 separate items, but rather is the second item a logical consequence of the first. Then I would suggest to remove "Firstly" and to replace "Secondly" by "Therefore"

Done (Indeed excellent proposal)

- line 223: mention that these are "biased residuals"

Done text reads now: "the - biased - residuals"

- Eq. (3): there is one "+" too many

Done

- Figure 5 caption: "... for (left) $B=0T$ and (right) $B=1T$ ", same for Fig. 6

Done

- line 267: sigma => \sigma

Done

- line 284: check language in "deformations in the pixel plane deformation"

Done

- line 289: In their reply, the authors state that 8x16 pixels is wrong, as I realized in the first review. It is still not corrected here. In addition, "bins were grouped into 8x16 pixels" is not understandable. It should probably rather read "groups of 16x16 pixels were combined into one bin"

This should have been corrected already. Done adding this explanation.

- line 295: "upper corner edge" is not understandable; maybe one could direct the reader by values of the coordinates, e.g. $y > 2500$, $x > 500$?

Added "to the right upper corner edge" looking back at Fig the reader can find the location of chip16

- line 296: "inhomogeneities"

Done

- line 296: add "...pillars, where the..."

Done

- line 308: the expression "dike" is used here for the first time without explanation. Probably this should be defined in Sec. 2.

Rephrased: 'Due to the presence a so-called dike - that was created in the TPX3 post-processing to protect the edges of the TPX3 chip - '

- line 309: "became" => "were"

Done

- line 310f: "the chip" => "each chip" (2x)

Done

- Figure 9 caption: "in the (top) pixel and (bottom) drift plane", same for Fig.10

Done

- line 334: "bins were grouped into 16x16 pixels" is not understandable, see above.

Corrected

- line 338: "upper corner edge", see above

Done

-line 348 and 358: "deformation studies"

Done

- Figure 11 caption: "(left) B=0T and (right) B=1T data"

Done

- line 380: comma before "respectively"

Done

- line 414: I suggest to add a footnote to contact the author if interested

Done

Declaration of interests

The authors declare that they have no known competing financial interests or personal relationships that could have appeared to influence the work reported in this paper.

The authors declare the following financial interests/personal relationships which may be considered as potential competing interests:

1 Towards a Pixel TPC part I: construction and test of a
2 32-chip GridPix detector

3 M. van Beuzekom^a, Y. Bilevych^b, K. Desch^b, S. van Doesburg^a,
4 H. van der Graaf^a, F. Hartjes^a, J. Kaminski^b, P.M. Kluit^a,
5 N. van der Kolk^a, C. Ligtenberg^a, G. Raven^a, J. Timmermans^a

6 ^a*Nikhef, Science Park 105, 1098 XG Amsterdam, The Netherlands*

7 ^b*Physikalisches Institut, University of Bonn, Nussallee 12, 53115 Bonn,*
8 *Germany*

9 **Abstract**

10 A Time Projection Chamber (TPC) module with 32 GridPix chips was con-
11 structed and the performance was measured using data taken in a testbeam
12 at DESY in 2021. The GridPix chips each consist of a Timepix3 ASIC
13 (TPX3) with an integrated amplification grid and have a high efficiency of
14 about 85% to detect single ionisation electrons. In the testbeam setup, the
15 module was placed in between two sets of Mimosas26 silicon detector planes
16 that provided external high-precision tracking and the whole detector setup
17 was slid into the PCMAG magnet at DESY. The TPC could be operated
18 reliably and used a 93.6/5.0/1.4 gas mixture (by volume) of Ar/iC₄H₁₀/CO₂
19 with a small amount of oxygen and water vapour. The analysed data were
20 taken at electron beam momenta of 5 and 6 GeV/c and at magnetic fields of
21 0 and 1 T.

22 The result for the transverse diffusion coefficient D_T is (287.2 ± 0.5)
23 $\mu\text{m}/\sqrt{\text{cm}}$ at $B = 0$ T and D_T (120.3 ± 0.5) $\mu\text{m}/\sqrt{\text{cm}}$ at $B = 1$ T. The
24 longitudinal diffusion coefficient D_L is measured to be (251 ± 14) $\mu\text{m}/\sqrt{\text{cm}}$

*Corresponding author, Telephone: +31 20 592 2000
Preprint submitted to Nuclear Instruments and Methods A
Email address: s01@nikhef.nl (P.M. Kluit)

25 at $B = 0$ T and $(224 \pm 14) \mu\text{m}/\sqrt{\text{cm}}$ at $B = 1$ T. Results for the tracking
26 systematical uncertainties in xy (pixel plane) were measured to be smaller
27 than $13 \mu\text{m}$ with and without magnetic field. The tracking systematical
28 uncertainties in z (drift direction) were smaller than $15 \mu\text{m}$ ($B = 0$ T) and
29 $20 \mu\text{m}$ ($B = 1$ T).

30 *Keywords:*

31 Micromegas, gaseous pixel detector, micro-pattern gaseous detector,
32 Timepix, GridPix, pixel time projection chamber

33 1. Introduction

34 Earlier publications on a single chip [1] and four chip (quad) GridPix de-
35 tectors [2] showed the potential of the GridPix technology and the large range
36 of applications for these devices [3]. In particular, it was demonstrated that
37 single ionisation electrons can be detected with high efficiency and accuracy,
38 allowing excellent 3D track position measurements and particle identification
39 based on the number of electrons and clusters.

40 As a next step towards a Pixel Time Projection Chamber for a future
41 collider experiment [4, 5], a module consisting of 32 GridPix chips based on
42 the TPX3 chip was constructed.

43 A GridPix detector consists of a CMOS pixel TPX3 chip [6] with inte-
44 grated amplification grid added by photo-lithographic - Micro-electromechanical
45 Systems (MEMS) - post-processing techniques. The TPX3 chip can be op-
46 erated with a low threshold of $515 e^-$, and has a low equivalent noise charge
47 of about $70 e^-$. The GridPix single chip and quad detectors have a very
48 fine granularity of $55 \times 55 \mu\text{m}^2$ with 256×256 pixels per chip. The device has

49 a high efficiency of about 85% - discussed in this paper - to detect single
50 ionisation electrons.

51 Based on the experience gained with these detectors a 32-GridPix detector
52 module - consisting of 8 quad detectors - was built. A drift box defining the
53 electric field and gas envelope was constructed. A read out system for up
54 to 128 chips with 4 multiplexers read out by one Speedy Pixel Detector
55 Readout (SPIDR) board [7, 8] was designed. After a series of tests using
56 the laser setup [9] and cosmics in the laboratory at Nikhef, the detector was
57 taken to DESY for a two week testbeam campaign.

58 At DESY, the 32-chip detector was placed in between two sets of Mi-
59 mosa26 silicon detector planes and mounted on a movable stage. The whole
60 detector setup was slid into the centre of the PCMAG magnet at DESY.
61 A beam trigger was provided by scintillator counters. The data reported
62 here were taken at different stage positions and electron beam momenta of
63 5 and 6 GeV/c and at magnetic fields of 0 and 1 T. The performance of the
64 32-GridPix detector module was measured using these data sets.

65 In this paper, part I of the results will be presented with the main focus on
66 the detector spatial resolution and tracking performance. A second follow-up
67 paper will discuss the dE/dx (or dN/dx) and other results.

68 **2. The 32-GridPix detector module**

69 A 32-GridPix detector module was built using the quad detector module
70 [2] as a basic building block. The quad module consists of four GridPix chips
71 and is optimised for a high fraction of sensitive area of 68.9%. The external
72 dimensions are 39.60 mm \times 28.38 mm. The four chips which are mounted

73 on a cooled base plate (COCA), are connected with wire bonds to a common
74 central 6 mm wide PCB. A 10 mm wide guard electrode is placed over the
75 wire bonds 1.1 mm above the aluminium grids, in order to prevent field
76 distortions of the electric drift field. The guard electrode is the main inactive
77 area, and its dimensions are set by the space required for the wire bonds.
78 On the back side of the quad module, the PCB is connected to a low voltage
79 regulator. The aluminium grids of the GridPix detectors are connected by
80 80 μm insulated copper wires to a high voltage (HV) filtering board. The
81 quad module consumes about 8 W of power of which 2 W is used in the LV
82 regulator.

83 Eight quad modules were embedded in a box, resulting in a GridPix
84 detector module with a total of 32 chips. A schematic 3-dimensional drawing
85 of the detector is shown in Figure 1. A schematic drawing of the quad
86 detectors in the module is shown in Figure 2, where also the beam direction
87 is indicated.

88 The internal dimensions of the box are 79 mm along the x -axis, 192 mm
89 along the y -axis, and 53 mm along the z -axis (drift direction), and it has a
90 maximum drift length (distance between cathode and read out anode) of 40
91 mm. The drift field is shaped by a series of parallel CuBe field wires of 75
92 μm diameter with a wire pitch of 2 mm. Guard strips are located on all of
93 the four sides of the active area. In addition, six guard wires - shown with
94 dashed lines (one colored red) in Figure 2 - are suspended over the boundaries
95 of the chips, to minimise distortions of the electric drift field. The wires are
96 located at a distance of 1.15 mm from the grid planes, and their potential is
97 set to the drift potential at this drift distance. The box has two 50 μm thick

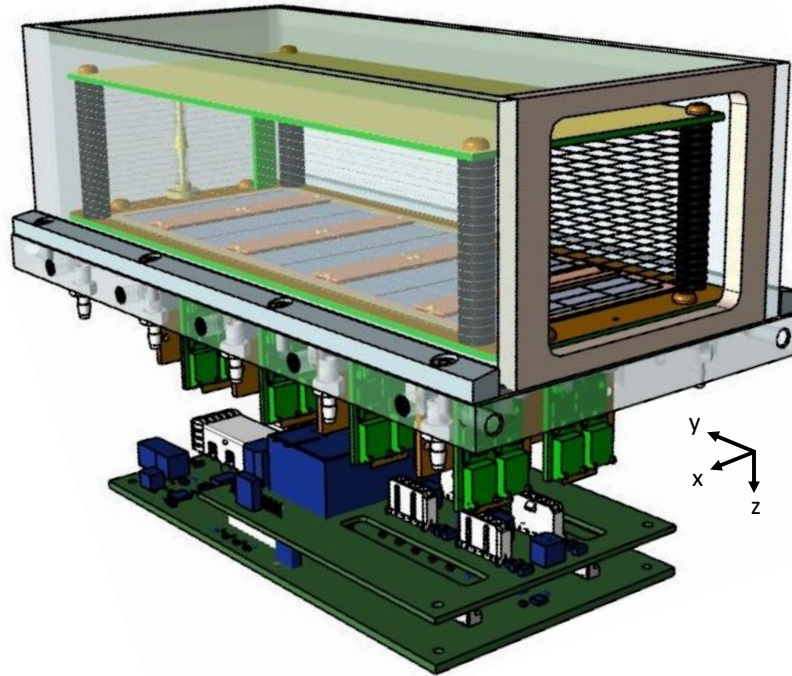


Figure 1: Schematic 3-dimensional rendering of the 32-GridPix module detector for illustration purposes.

98 Kapton windows to allow the beam to pass with minimal multiple scattering.
99 The gas volume of 780 ml is continuously flushed at a rate of ~ 50 ml/min
100 (about 4 volumes/hour) with premixed T2K TPC gas. This gas is a mixture
101 consisting of 95% Ar, 3% CF_4 , and 2% iC_4H_{10} suitable for large TPCs because
102 of the low transverse diffusion in a magnetic field and the high drift velocity.
103 The data acquisition system of the quad module was adopted to allow for
104 reading out multiple quad detectors. A multiplexer card was developed that
105 handles four quad detectors or 16 chips and combines the TPX3 data into
106 one data stream. For the 32-GridPix module two multiplexers are connected
107 to a SPIDR board that controls the chips and read out process. The read

108 out speed per chip is 160 Mbps and for the multiplexer 2.56 Gbps: this
 109 corresponds to a maximum rate of 21 MHits/s. For each pixel the precise
 110 Time of Arrival (ToA) using a 640 MHz TDC and the time over threshold
 111 (ToT) are measured.

112 3. Experimental setup

113 In preparation of the two weeks DESY testbeam campaign, a support
 114 frame was designed to move the 32-chip GridPix detector module in the
 115 plane perpendicular to the beam by a remotely controlled stage such that
 116 the whole detector volume could be probed. The module was mounted upside
 117 down with respect to Figure 1 to allow access to the electronics from above.

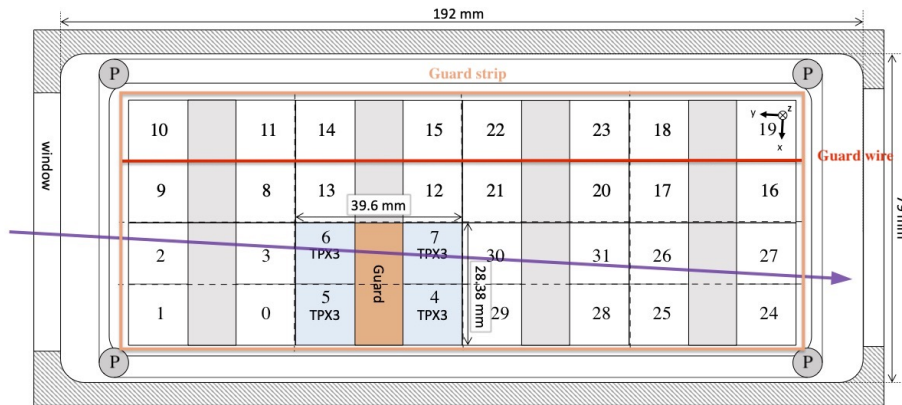


Figure 2: Schematic drawing of the 32-GridPix module detector with one example quad as viewed from the top of the quad detectors. The chips are numbered and the beam direction is shown in purple. A guard electrode of a quad detector is shown in orange. The four surrounding guard strips are shown -not to scale- in orange. Six guard wires - are shown with dashed lines (one colored red) and the pillars of the drift box are shown as circles with a P in the centre.

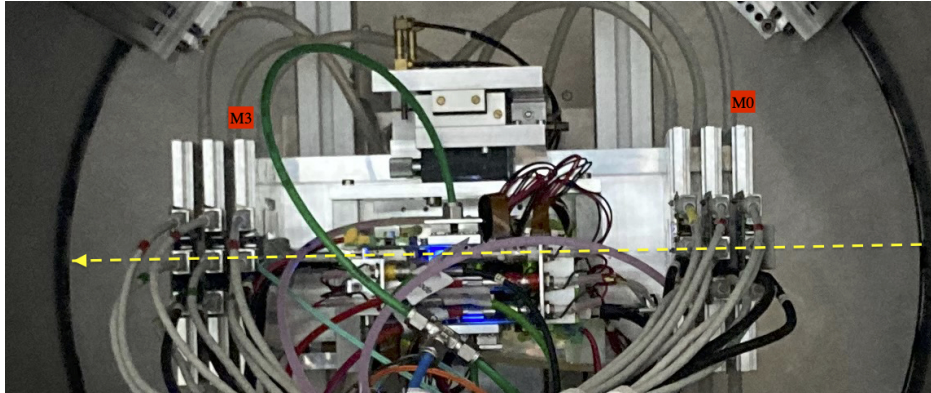


Figure 3: Photo of the detector setup - side view - at the centre of the PCMAG magnet (the circular contour). The Mimosa26 planes M0 and M3 are indicated in red as well as the beam direction (yellow).

118 The support frame also held three Mimosa26 silicon detector planes [10] -
119 with an active area of $(21.2 \text{ mm} \times 10.6 \text{ mm})$ - placed in front of the detector
120 and three Mimosa26 planes behind the detector. At DESY, the Mimosa26
121 silicon detector planes were provided by the testbeam coordinators. The
122 whole detector setup was slid towards the centre of the PCMAG magnet
123 at the DESY II testbeam facility [10]. A beam trigger was provided by a
124 double scintillator counter coincidence. The data were taken at different
125 stage positions to cover the whole sensitive TPC volume. Runs with electron
126 beam momenta of 5 and 6 GeV/c and at magnetic fields of 0 and 1 T were
127 analysed.

128 A photograph of the detector setup in the PCMAG magnet is shown in
129 Figure 3. The stage positions of the TPC module with respect to the beam
130 and the Mimosa26 planes can be adjusted.

131 The experimental and environmental parameters such as temperature,

132 pressure, gas flow and oxygen content were measured and logged by a Win-
 133 dows operated slow control system. The experimental parameters are sum-
 134 marised in Table 1. The chips were cooled by circulating Glycol through
 135 the cooling channels in the module carrier plate. The cooling blocks of the
 136 multiplexers were further cooled by blowing pressurised air on them.

Table 1: Overview of the experimental parameters. The ranges indicate the variation over the data taking period

Number of analysed runs at $B=0$ (1) T	6 (8)
Run duration	10-90 minutes
Number of triggers per run	3-100 k
E_{drift}	280 V/cm
V_{grid}	340 V
Threshold	550 e ⁻
Gas temperature	303.3-306.6 K
Pressure	1011 – 1023 mbar
Oxygen concentration	240 - 620 ppm
Water vapour concentration	2000 - 7000 ppm

137 The data was produced in four main data streams: one stream produced
 138 by the Mimosa26 telescope, two data streams by the two Timepix multiplex-
 139 ers and one trigger stream. The double scintillator coincidence provided a
 140 trigger signal to the Trigger Logic Unit (TLU) [11] that sends a signal to the
 141 telescope read out and the trigger SPIDR. The data acquisition systems of
 142 the telescope and trigger SPIDR injected a time stamp into their respective
 143 data streams. Hits from the Mimosa26 planes were collected with a sliding

144 window of $-115 \mu\text{s}$ to $230 \mu\text{s}$ around the trigger time. The data acquisition
145 of the multiplexer and the trigger SPIDR were synchronised at the start of
146 the run. By comparing the time stamps in these streams, telescope tracks
147 and TPC tracks could be matched. Unfortunately, the SPIDR trigger had
148 - due to a cabling mistake at the output of the TLU - a common 25 ns flat
149 time jitter.

150 After a short data taking period one of the chips (nr 11) developed a
151 short circuit and the HV on the grid of the chip was disconnected. After the
152 testbeam data taking period the module was repaired in the clean room in
153 Bonn.

154 4. Analysis

155 4.1. Telescope track reconstruction procedure

156 The data of the telescope is decoded and analysed using the Corryvreckan
157 software package [12]. The track model used for fitting was the General
158 Broken Lines (GBL) software [14]. The code was extended and optimised to
159 fit curved broken lines for the data with magnetic field. The telescope planes
160 were iteratively aligned using the standard alignment software provided by
161 the package. The single point Mimosas26 resolution is $4 \mu\text{m}$ in x and $6 \mu\text{m}$
162 in z (drift direction) [10].

163 Telescope tracks were required to have hits in at least 5 out of the 6 planes
164 and a total χ^2 of better than 25 per degree of freedom. The uncertainties on
165 the telescope track prediction in the middle of the GridPix detector module
166 are dominated by multiple scattering. The amount of multiple scattering
167 was estimated by comparing the predictions from the two telescope arms for

168 6 GeV/c tracks at $B = 0$ T. The expected uncertainty in x and z is $26 \mu\text{m}$
169 on average.

170 4.2. TPC Track reconstruction procedure

171 GridPx hits are selected requiring a minimum time over threshold ToT
172 of $0.15 \mu\text{s}$. The drift time is defined as the measured time of arrival minus
173 the trigger time recorded in the trigger SPIDR data stream minus a fixed t_0
174 (the drift time at zero drift). The drift time was corrected for time walk [2]
175 using the measured time over threshold (ToT in units of μs) and the formula
176 (1):

$$\delta t = \frac{18.6(ns \mu s)}{\text{ToT} + 0.1577(\mu s)}. \quad (1)$$

177 Furthermore, small time shift corrections - with an odd-even and a $16 \times$ pixels
178 structure - coming from the TPX3 clock distribution were extracted from the
179 data and applied.

180 The z drift coordinate was calculated as the product of the drift time
181 and the drift velocity. This implies that $z_{\text{drift}} = -z$ as defined in Figure 1.
182 GridPix hits outside an acceptance window of 30 mm wide in x and 15 mm
183 wide in z , corresponding to the size of the entrance window, were not used
184 in the track finding and reconstruction. Based on a Hough transform an
185 estimate of the TPC track position and angles in the middle of the module
186 (at $y = 1436$ pixels) were obtained. This estimate was used to collect the hits
187 around the TPC track and fit the track parameters. For this fit a linear (for
188 $B = 0$ T data) or a quadratic track (for $B = 1$ T data) model was used. In
189 the fit, the expected uncertainties per hit σ_{xy} and σ_z were used. The expected

Table 2: Table with track/event selection cuts

Track/Event Selection
$ x_{\text{TPC}} - x_{\text{telescope}} < 0.3 \text{ mm}$
$ z_{\text{TPC}} - z_{\text{telescope}} < 2 \text{ mm}$
$ dx/dy_{\text{TPC}} - dx/dy_{\text{telescope}} < 4 \text{ mrad}$
$ dz/dy_{\text{TPC}} - dz/dy_{\text{telescope}} < 2 \text{ mrad}$

190 uncertainties were derived using the parametrisations discussed in section 5.
 191 The fit was iterated three times to reject outlier hits at respectively 10, 5
 192 and 2.5 sigma. A TPC track was required to have at least 100 hits in each
 193 multiplexer. At least 25% of the total number of hits should be on track and
 194 the χ^2 per degree of freedom had to be less than 3 in xy and zy . All track
 195 parameters were expressed at a plane in the middle of the TPC module.

196 The calibration and alignment of the detector was done using high quality
 197 tracks for which the track selections are summarised in Table 2.

198 The drift velocity was calibrated per run by fitting a linear function to
 199 the z (predicted from the telescope track at the measured TPC hit position)
 200 versus the measured drift time in the TPC. For the $B = 0$ T runs it varies
 201 between 61.6 and 63.0 $\mu\text{m}/\text{ns}$. For the $B = 1$ T runs it is between 57.2 and
 202 59.1 $\mu\text{m}/\text{ns}$. The variation comes mainly from the changes in the relative
 203 humidity of the gas volume due to small leaks.

204 The individual TPX3 chips were iteratively aligned fitting a shift in x (z)
 205 and two slopes $dx(z)/dx(y)$. The alignment was done per run, because the
 206 detector was moved in x and/or z for each run. The fitted slopes were also
 207 corrected for small shifts and rotations (3D) in the nominal chip position.

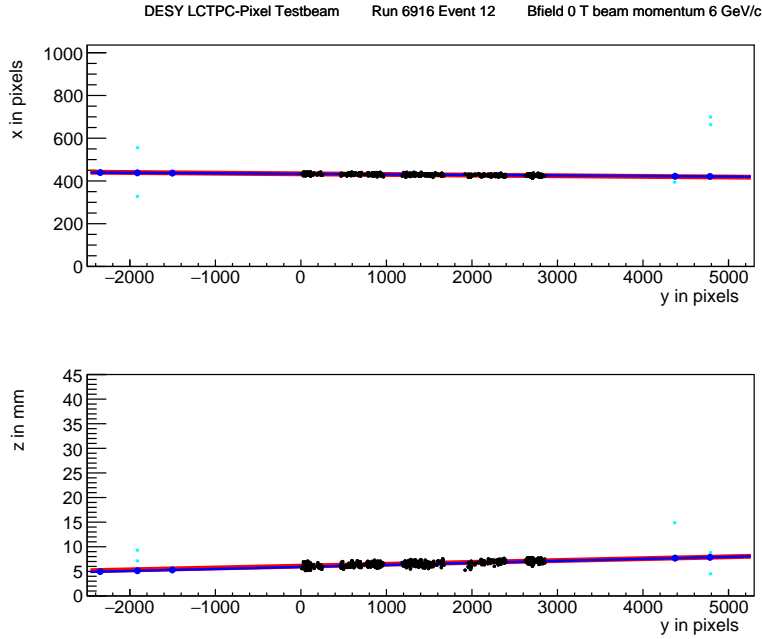


Figure 4: An event display for run 6916 without B field, with in total 1293 TPC hits (black dots) in the (top) precision plane (x, y) and (bottom) drift plane (z drift, y). The fitted TPC track (red line) with 1130 hits on track and the telescope track (blue line) with 5 Mimoso26 planes (blue hits) on track are shown. In green the off track Mimoso26 hits are shown.

208 An example event from run 6916 without B field with a TPC and a
 209 telescope track is shown in Figure 4. The TPC is located between $y = 0$ and
 210 2872 pixels. Three Mimoso26 planes are located at $y < -1000$ and three at
 211 $y > 4000$ pixels.

212 5. Hit resolutions

213 The track residual in xy is defined as the closest distance - defined as the
 214 2D xy projection of the 3D distance - between the hit at the center of the

215 pixel and the track. The residual in z is calculated at this point of closest
 216 approach. The single-electron hit resolutions in xy and z will be extracted
 217 from the track residuals. In order to study the single-electron resolution
 218 for the data with and without magnetic field, additional selections on the
 219 telescope and TPC tracks were applied. Due to the trigger time jitter of 25
 220 ns (corresponding to 1.5 mm drift), the prediction of the telescope track in
 221 z must be used as the reference for z . Therefore the z hits of the TPC track
 222 were fitted to correct for the common time shift and the - biased - z residuals
 223 were calculated with respect to the fitted TPC track. In the xy plane the
 224 residuals of TPC hits with respect to the telescope track were used to extract
 225 the single-electron resolution in xy . For the resolution studies, runs at three
 226 different z stage positions of the TPC were selected where the beam gave
 227 hits in the central chips. The data of 14 central chips (9, 12, 21, 20, 17, 16,
 228 2, 3, 6, 7, 30, 31, 26 and 27) were used. Two chips (8 and 13) were left out
 229 because of the E field deformations caused by the short circuit in chip 11.

230 5.1. Hit resolutions in the pixel plane

231 The residual of the hits in the pixel plane (xy) was measured as a function
 232 of the predicted drift position (z_{drift}). Tracks were selected that crossed the
 233 fiducial region defined by the central core of the beam. Hits were removed
 234 in a region of 20 pixels near the chip edges in x . The spread on the residual
 235 in xy for an ionisation electron is given by:

$$\sigma_{xy}^2 = \sigma_{\text{track}}^2 + \frac{d_{\text{pixel}}^2}{12} + D_T^2(z_{\text{drift}} - z_0), \quad (2)$$

236 where σ_{track} is the uncertainty from the track prediction, d_{pixel} is the pixel
 237 pitch size, z_0 is the position of the grid, and D_T is the transverse diffusion

238 coefficient. The last two terms correspond to the single-electron detector
 239 resolution (squared). The resolution at zero drift distance $d_{\text{pixel}}/\sqrt{12}$ was
 240 fixed to $15.9 \mu\text{m}$ and σ_{track} to $30 \mu\text{m}$ for $B = 0 \text{ T}$ and $42 \mu\text{m}$ for $B =$
 241 1 T data. The uncertainty on the track prediction was measured and is
 242 larger than the Mimosa plane resolution because of multiple scattering in
 243 the sensors and in the entrance and exit windows.

244 The expression (2) - leaving z_0 and D_T as free parameters - is fitted
 245 to the $B = 0 \text{ T}$ data shown in Figure 5. The fit gives a transverse diffusion
 246 coefficient D_T of $(287.2 \pm 0.5) \mu\text{m}/\sqrt{\text{cm}}$. The measured value is in agreement
 247 with the value of $287 \mu\text{m}/\sqrt{\text{cm}} \pm 4\%$ predicted by the gas simulation software
 248 Magboltz 11.9 [15]. The values of the diffusion coefficients depend on the
 249 humidity that was not precisely measured during the testbeam. The humidity
 250 strongly affects the drift velocity. Therefore the drift velocity prediction from
 251 Magboltz was used to determine the water content per run and predictions
 252 for the diffusion coefficients could be obtained.

253 A fit to the $B = 1 \text{ T}$ data, also shown in Figure 5, gives a transverse
 254 diffusion coefficient D_T of $(120.3 \pm 0.5) \mu\text{m}/\sqrt{\text{cm}}$. The measured value is in
 255 agreement with the value of $119 \mu\text{m}/\sqrt{\text{cm}} \pm 2\%$ predicted by Magboltz.

256 5.2. Hit resolution in the drift plane

257 The spread on the residual in z of the ionisation electrons σ_z is given by:

$$\sigma_z^2 = \sigma_{\text{track}}^2 + \sigma_{z_0}^2 + D_L^2(z_{\text{drift}} - z_0), \quad (3)$$

258 where σ_{track} is the expected track uncertainty, σ_{z_0} the detector resolution at
 259 zero drift distance and D_L the longitudinal diffusion constant. The last two
 260 terms in the equation correspond to the single-electron detector resolution

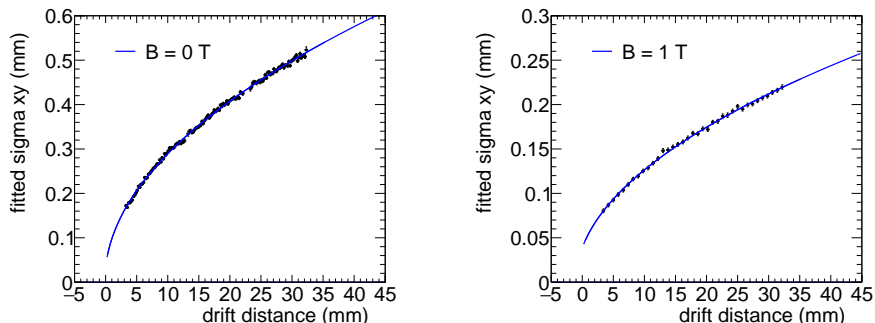


Figure 5: Measured spread on the residuals in the pixel plane (black points) for (left) $B = 0$ T and (right) $B = 1$ T, fitted with equation (2) (blue line).

261 (squared). Only tracks crossing the fiducial region - defined by the central
 262 core of the beam - were accepted and hits with a ToT value above $0.6 \mu\text{s}$
 263 were selected. Because of the time jitter, the fitted TPC track is used for the
 264 drift residuals. For z_{drift} the telescope prediction at the hit was used. The
 265 expected uncertainty on TPC track prediction is propagated and amounts to
 266 $50 \mu\text{m}$ at $z = z_0$. The systematic uncertainty on σ_{track} is estimated to be 25
 267 μm .

268 The expression (3) - leaving σ_{z_0} and D_L as free parameters - is fitted
 269 to the $B = 0$ T data shown in Figure 6. The value of z_0 was fixed to the
 270 result of the fit in the xy plane. The value of σ_{z_0} was measured to be 129
 271 μm . The longitudinal diffusion coefficient D_L was determined to be $(251$
 272 ± 1 (stat) ± 14 (sys)) $\mu\text{m}/\sqrt{\text{cm}}$, which is higher than the expected value
 273 $236 \pm 3 \mu\text{m}/\sqrt{\text{cm}}$ from a Magboltz calculation [15]. The quoted systematic
 274 uncertainty on D_L is rather large and obtained from a fit using $\sigma_{\text{track}} = 25$
 275 μm .

276 A fit to the $B = 1$ T data shown in Figure 6 gives a longitudinal diffusion

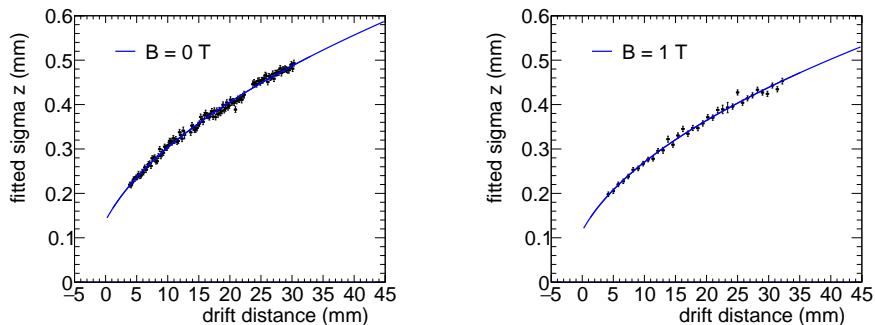


Figure 6: Measured spread on the residuals in the drift plane for hits with a ToT above $0.60 \mu\text{s}$ for (left) $B = 0 \text{ T}$ and (right) $B = 1 \text{ T}$. The data are fitted with the expression of equation (3).

277 coefficient D_L of $(224 \pm 2 \text{ (stat)} \pm 14 \text{ (sys)}) \mu\text{m}/\sqrt{\text{cm}}$. The measured value
 278 is lower than the value of $(245 \pm 4) \mu\text{m}/\sqrt{\text{cm}}$ predicted by Magboltz. The
 279 fitted value of σ_{z0} was $114 \mu\text{m}$.

280 5.3. Deformations in the pixel and drift plane

281 It is important to measure possible deformations in the pixel (xy) and
 282 drift (z) plane to quantify the tracking precision. For the construction of
 283 a large Pixel TPC, deformations in the pixel plane should be controlled to
 284 better than typically $20 \mu\text{m}$ because these affect the momentum resolution.
 285 The mean residuals in the pixel and drift planes are shown in Figure 7 for
 286 the $B = 0 \text{ T}$ data set using a large set of runs to cover the whole module.
 287 The residuals were calculated with respect to the telescope track prediction.
 288 Because of limited statistics, groups of 16×16 pixels were combined into one
 289 bin. Bins with less than 100 hits are left out and residuals larger (smaller)
 290 than $+(-)100 \mu\text{m}$ are shown in red (blue).

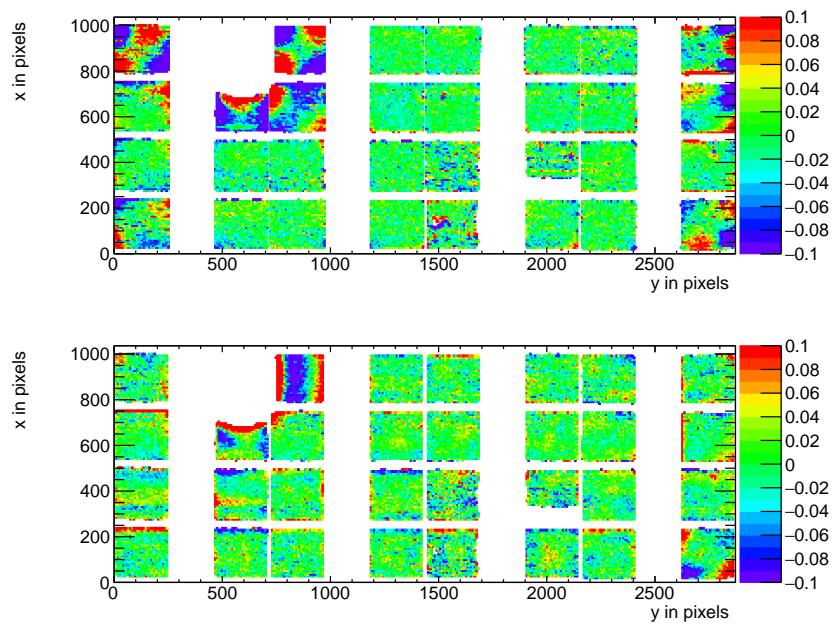


Figure 7: Mean residuals (color coded in mm) in the pixel (top) and drift (bottom) plane for $B = 0$ T data at the expected hit position.

291 A few critical areas can be observed in Figure 7: the region around chip 11
 292 is affected (chips 14, 8 and 13), because the grid of chip 11 was disconnected.
 293 Deformations are present at the four corners of the drift box (chips 1, 10,
 294 19 and 24) and close to the right upper corner edge (chip 16) of the drift
 295 box. These come from inhomogeneities in the drift field near the supporting
 296 pillars, where the field wires are too close to the chip to provide a constant
 297 electric field. It was concluded that for the deformation studies the hits of
 298 these nine chips have to be removed. The track fit was redone leaving these
 299 hits out of the fit, such that they could not bias and affect the results. Note
 300 that a bias in the mean residual at the edge of the chips is expected to be
 301 present for an ideal detector because of the finite coverage and the diffusion
 302 in the drift process.

303 In order to reduce the statistical fluctuations and quantify the tracking
 304 precision, the pixels were regrouped into larger bins respecting the module
 305 geometry. After the regrouping procedure, a module plane with $(4 \times 256) \times 256$
 306 bins is obtained, as shown in Figure 8 ¹. Bins have a size of 16×16 pixels and
 307 bins with less than 1000 entries are not shown. Due to the presence a so-called
 308 dike - that was created in the TPX3 post-processing to protect the edges of
 309 the TPX3 chip - pixels at the edge of the chip were covered and inefficient.
 310 Therefore, the region of 5 pixels in y near the edge of each chip was removed.
 311 For the drift coordinate studies, a region of 10 pixels near the edge of each

¹The mathematical procedure is defined as follows. The original mean residual - before rebinning - is given by $\text{residual}(i,j)$ where i runs horizontally and j vertically. The rebinned result for the $\text{residual}(4 \times 256, 256)$ is equal to $\text{residual}(i \% 1024, j \% 256)$. The mean $\text{residual}(256, 4 \times 256)$ - discussed later in the paper - is equal to $\text{residual}(i \% 256, j)$.

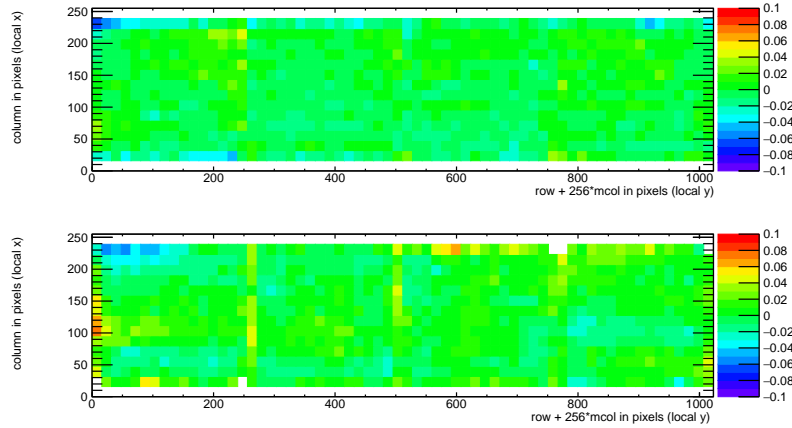


Figure 8: Mean residuals (color coded in mm) in the pixel (top) and drift plane (bottom) for $B = 0$ T data at the expected hit position.

312 chip in x and y was removed. The total number of measurements (bins) in
 313 xy is 895 and in z 892. One can observe that in the module plane no clear
 314 systematic deviations are present and conclude that the guard wire voltages
 315 were on average well tuned. Note that in the quad detector module we had
 316 no guard wires and deformation corrections had to be applied [2]. The r.m.s.
 317 of the distribution of the measured mean residual over the surface in the
 318 pixel plane is $11 \mu\text{m}$ and in the drift plane $15 \mu\text{m}$. Similarly, regrouping the
 319 module in a plane with $256 \times (4 \times 256)$ pixel bins, yielded a r.m.s. in the pixel
 320 plane of $13 \mu\text{m}$ and $13 \mu\text{m}$ in the drift coordinate. The expected statistical
 321 error - obtained by propagating the uncertainties on the residuals - in xy is
 322 $4 \mu\text{m}$ and in z $5 \mu\text{m}$.

323 In the $B = 1$ T data set, the electrons will drift mainly along the magnetic
 324 field lines. Deformations are in that case due to e.g. the non-alignment of the
 325 electric and magnetic field, giving $E \times B$ effects. Unfortunately, the statistics

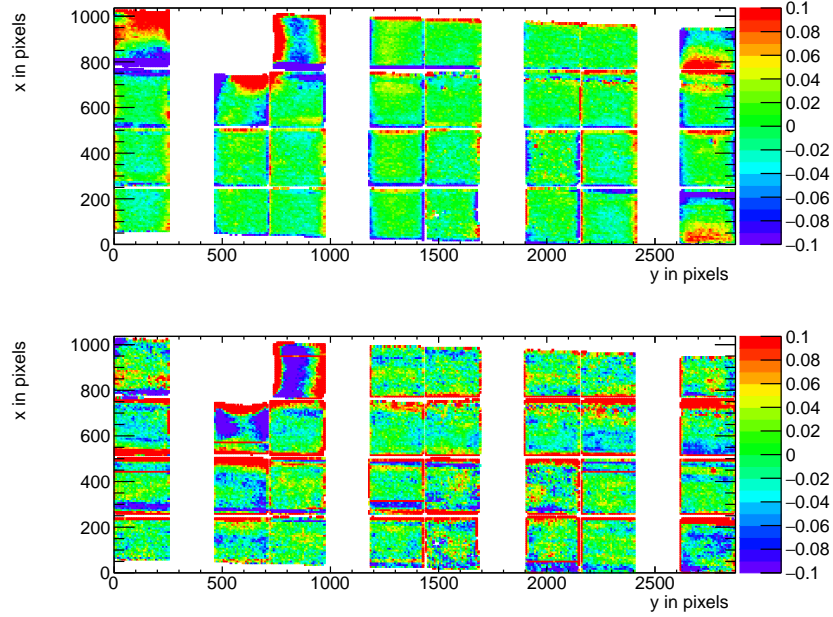


Figure 9: Mean residuals (color coded in mm) in the pixel (top) and drift plane (bottom) for $B = 1$ T data at the expected hit position.

326 of the telescope tracks that have a matched TPC track was insufficient and
 327 did not cover the full TPC module plane. Therefore the larger statistics of
 328 matched and unmatched TPC tracks was used. TPC tracks were required
 329 to pass angular selection cuts (dx/dy between -40 and -20 mrad and dz/dy
 330 between 0 and 14 mrad) and a momentum cut ($p > 2$ GeV/c and $q < 0$).

331 The mean residuals in the pixel and drift planes are shown in Figure 9 for
 332 the $B = 1$ T data set using a large set of runs to cover the whole module. The
 333 (biased) residuals were calculated with respect to the TPC track prediction.
 334 Because of limited statistics, bins were grouped into 16×16 pixels. Bins with
 335 less than 100 hits are left out and residuals larger (smaller) than $+(-)100 \mu\text{m}$
 336 are shown in red (blue).

337 In Figure 9 the critical areas discussed above - around chip 11, the four
338 corner chips and chip 16 in the right upper corner edge - can be clearly
339 observed. For the deformation studies, the hits of these nine chips were
340 removed. The TPC track fit was redone leaving these hits out of the fit,
341 thus that they could not bias and affect the results. The TPC plane is well
342 covered, although one can observe that due to the angle of the beam in the
343 xy plane the chips in the upper right and lower left corners are not fully
344 covered.

345 In order to reduce the statistical fluctuations and quantify the tracking
346 precision, the module was again regrouped in $(4 \times 256) \times 256$ pixels as de-
347 scribed above, as shown in Figure 10. Bins have a size of 16×16 pixels and
348 bins with less than 1000 entries are not shown. Similar to the no-field defor-
349 mation studies, acceptance cuts had to be applied. The region of 16 pixels in
350 y near the edge of the chips was removed. For the drift coordinate studies,
351 in addition a region of 10 pixels in x near the edge of the chip was removed.
352 The total number of measurements (bins) in xy is 896 and in z 896. One can
353 observe that in the module plane no clear systematic deviations are present.
354 The r.m.s. of the distribution of the measured mean residual over the surface
355 in the pixel plane is $13 \mu\text{m}$ and in the drift plane $19 \mu\text{m}$. Similarly, regroup-
356 ing the module in $256 \times (4 \times 256)$ pixel bins, yielded a r.m.s. in the pixel plane
357 of $11 \mu\text{m}$ and $20 \mu\text{m}$ in the drift coordinate. The expected statistical error
358 in xy is $2 \mu\text{m}$ and in z $3 \mu\text{m}$.

359 In summary, the deformation studies for the $B = 0$ and 1 T data demon-
360 strate that the systematical uncertainties in xy are smaller than $13 \mu\text{m}$ with
361 and without magnetic field. The systematical uncertainties in z were smaller

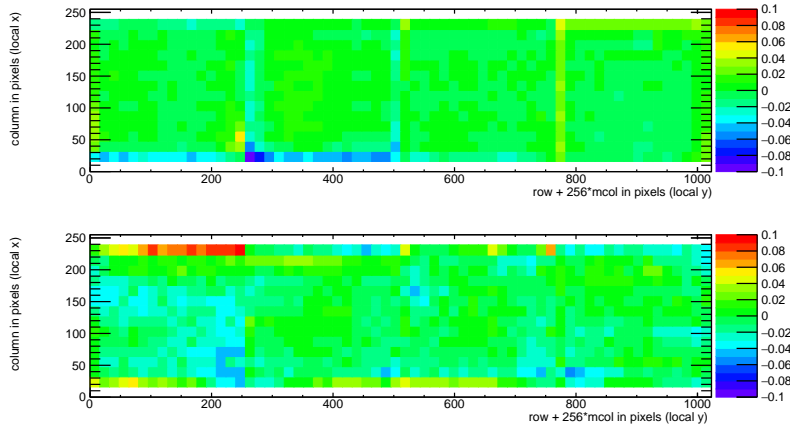


Figure 10: Mean residuals (color coded in mm) in the pixel and drift plane for $B = 1\text{T}$ data at the expected hit position.

362 than $15\ \mu\text{m}$ ($B = 0\ \text{T}$) and $20\ \mu\text{m}$ ($B = 1\ \text{T}$).

363 5.4. Tracking resolution

364 A selected TPC track in the $B = 0\ \text{T}$ data has on average 1000 hits. The
 365 tracking precision in the middle of the TPC (at $y = 1436$ pixels) was derived
 366 on a track-by-track basis, by propagating the pixel TPC hit uncertainties. It
 367 was found to be on average $9\ \mu\text{m}$ in the precision plane and $13\ \mu\text{m}$ in z . The
 368 angular resolution in dx/dy was on average $0.19\ \text{mrad}$ and for dz/dy 0.25
 369 mrad . It is clear that the position resolution in the TPC in the precision
 370 and drift coordinates is impressive for a track length of (only) $158\ \text{mm}$.
 371 The values are smaller than the uncertainty on the track prediction from
 372 the silicon telescope of $26\ \mu\text{m}$ in x and z on average that is dominated by
 373 multiple scattering.

374 **6. Single electron efficiency**

375 The distribution of the number of TPC track hits per chip - without
376 requiring a matched telescope track - are shown in Figure 11 for the data
377 without magnetic field and for the $B = 1$ T data. For the $B = 0$ T data, the
378 central chips 2,6,7,9,16,17,26 and 27 were selected. For the $B = 1$ T data,
379 the same chips plus chips 12,13,20 and 21 were selected.

380 The mean number of hits is measured to be 124 and 89 in the $B = 0$ T
381 and 1 T data sets, respectively. The most probable values are respectively
382 87 and 64. Note that the $B = 0$ T data have a much larger Landau-like tail
383 than the 1 T data. Also the fluctuations in the core of the distribution are
384 larger. The mean time over threshold (ToT) is $0.68 \mu\text{s}$ for the $B = 0$ T and
385 $0.86 \mu\text{s}$ at a $B = 1$ T data. A typical ToT distribution can be found in Figure
386 6 of [1] and Figure 5.5 of [4]. The time over threshold is related to the charge
387 after avalanche multiplication. This means that the mean deposited charge
388 per pixel is smaller for the 0 T data. The most probable value for the total
389 deposited charge is similar for both data sets. A possible explanation for
390 this behavior is that because of the reduced transverse diffusion in the $B =$
391 1 T data, the possibility of two primary electrons ending up in a single grid
392 hole is higher. The mean number of hits is in agreement with the prediction
393 of 106 electron-ion pairs for a 5 and 6 GeV/c electron at $B = 0$ T for the
394 T2K gas by [13], crossing 236 pixels or 12.98 mm and a detector running at
395 85% single-electron efficiency. The measured single-electron efficiency at this
396 working point is in agreement with the efficiency vs mean time over threshold
397 curve that was measured using a Fe source [4].

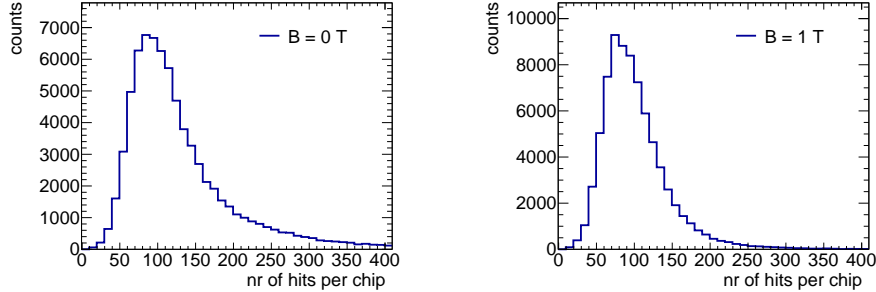


Figure 11: Distribution of the number of TPC track hits per chip for (left) $B = 0$ T and (right) $B = 1$ T data.

398 7. Conclusion and outlook

399 A TPC module with 32 GridPix chips was constructed and the perfor-
 400 mance was measured using data taken in a testbeam at DESY in 2021. The
 401 TPC could be operated reliably and used a 93.6/5.0/1.4 gas mixture (by vol-
 402 ume) of Ar/ i C₄H₁₀/CO₂ with a small amount of oxygen and water vapour.
 403 The analysed data were taken at electron beam momenta of 5 and 6 GeV/ c
 404 and at magnetic fields of 0 and 1 T.

405 The result for the transverse diffusion coefficient D_T is (287.2 ± 0.5)
 406 $\mu\text{m}/\sqrt{\text{cm}}$ at $B = 0$ T and D_T is $(120.3 \pm 0.5) \mu\text{m}/\sqrt{\text{cm}}$ at $B = 1$ T. The
 407 longitudinal diffusion coefficient D_L is measured to be $(251 \pm 14) \mu\text{m}/\sqrt{\text{cm}}$
 408 at $B = 0$ T and $(224 \pm 14) \mu\text{m}/\sqrt{\text{cm}}$ at $B = 1$ T. Results for the tracking
 409 systematical uncertainties in xy were measured to be smaller than 13 μm
 410 with and without magnetic field. The tracking systematical uncertainties in
 411 z were smaller than 15 μm ($B = 0$ T) and 20 μm ($B = 1$ T).

412 The mean number of hits is in agreement with the predictions of [13] and
 413 a detector running at 85% single-electron efficiency.

414 Not all data were analysed and users are welcome to study them using
415 the data sets on available on the Grid ².

416 The GridPix detector will be further tested and developed in view of a
417 TPC that will be installed in a heavy ion experiment at the EIC or other
418 future colliders. A follow-up paper is in preparation on the measured dE/dx
419 or dN/dx resolution and other performance topics.

420 **Acknowledgements**

421 This research was funded by the Netherlands Organisation for Scientific
422 Research NWO. The authors want to thank the support of the mechanical
423 and electronics departments at Nikhef and the detector laboratory in Bonn.
424 The measurements leading to these results have been performed at the Test
425 Beam Facility at DESY Hamburg (Germany), a member of the Helmholtz
426 Association (HGF).

427 **References**

- 428 [1] C. Ligtenberg, et al., Performance of a GridPix detector based
429 on the Timepix3 chip, Nucl. Instrum. Meth. A 908 (2018) 18–23.
430 arXiv:1808.04565, doi:10.1016/j.nima.2018.08.012.
- 431 [2] C. Ligtenberg, et al., Performance of the GridPix detector quad,
432 Nucl. Instrum. Meth. A 956 (2020) 163331. arXiv:2001.01540,
433 doi:10.1016/j.nima.2019.163331.

²For more information, please contact the corresponding author.

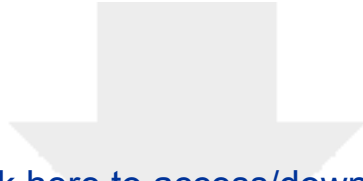
- 434 [3] J. Kaminski, Y. Bilevych, K. Desch, C. Krieger, M. Lupberger, GridPix
435 detectors - introduction and applications, Nucl. Instrum. Meth. A845
436 (2017) 233–235. doi:10.1016/j.nima.2016.05.134.
- 437 [4] C. Ligtenberg, A GridPix TPC read out for the ILD experiment at the
438 future International Linear Collider, Ph.D. thesis, Free University of
439 Amsterdam (2021). URL
440 https://www.nikhef.nl/pub/services/biblio/theses_pdf/thesis_C_Ligtenberg.pdf
- 441 [5] M. Lupberger, Y. Bilevych, H. Blank, D. Danilov, K. Desch, A. Hamann,
442 J. Kaminski, W. Ockenfels, J. Tomtschak, S. Zigann-Wack, To-
443 ward the Pixel-TPC: Construction and Operation of a Large Area
444 GridPix Detector, IEEE Trans. Nucl. Sci. 64 (5) (2017) 1159–1167.
445 doi:10.1109/TNS.2017.2689244.
- 446 [6] T. Poikela, J. Plosila, T. Westerlund, M. Campbell, M. De Gaspari,
447 X. Llopart, V. Gromov, R. Kluit, M. van Beuzekom, F. Zappone,
448 V. Zivkovic, C. Brezina, K. Desch, Y. Fu, A. Kruth, Timepix3: a 65K
449 channel hybrid pixel read out chip with simultaneous ToA/ToT and
450 sparse read out, JINST 9 (05) (2014) C05013.
451 URL <http://stacks.iop.org/1748-0221/9/i=05/a=C05013>
- 452 [7] J. Visser, M. van Beuzekom, H. Boterenbrood, B. van der Heijden, J. I.
453 Muñoz, S. Kulis, B. Munneke, F. Schreuder, SPIDR: a read-out system
454 for Medipix3 & Timepix3, Journal of Instrumentation 10 (12) (2015)
455 C12028. doi:10.1088/1748-0221/10/12/C12028.
- 456 [8] B. van der Heijden, J. Visser, M. van Beuzekom, H. Boterenbrood,

- 457 S. Kulis, B. Munneke, F. Schreuder, SPIDR, a general-purpose read out
458 system for pixel ASICs, JINST 12 (02) (2017) C02040. doi:10.1088/1748-
459 0221/12/02/C02040.
- 460 [9] F. Hartjes, A diffraction limited nitrogen laser for detector calibration in
461 high energy physics, Ph.D. thesis, University of Amsterdam (1990). URL
462 https://www.nikhef.nl/pub/services/biblio/theses_pdf/thesis_F_Hartjes.pdf
- 463 [10] R. Diener et al., The DESY II test beam facility, Nuclear Instru-
464 ments and Methods in Physics Research. Section A: Accelerators, Spec-
465 trometers, Detectors and Associated Equipment 922 (2019) 265–286.
466 arXiv:1807.09328, doi:10.1016/j.nima.2018.11.133.
- 467 [11] P. Baesso, D. Cussans, J. Goldstein, , Journal of Instrumentation 14 (09)
468 (2019) P09019–P09019. arXiv:2005.00310.
469 URL <https://doi.org/10.1088/1748-0221/14/09/p09019>
- 470 [12] D. Dannheim, K. Dort, L. Huth, D. Hynds, I. Kremastiotis, J. Kröger,
471 M. Munker, F. Pitters, P. Schütze, S. Spannagel, T. Vanat, M. Williams,
472 , Journal of Instrumentation 16 (03) (2021) P03008. doi:10.1088/1748-
473 0221/16/03/p03008. arXiv:2011.12730.
474 URL <https://doi.org/10.1088/1748-0221/16/03/p03008>
- 475 [13] R. Veenhof, Garfield - simulation of gaseous detectors, version 9, Refer-
476 ence W5050 (1984-2010).
477 URL <https://garfield.web.cern.ch>
- 478 [14] C. Kleinwort, General broken lines as advanced track fitting method,
479 Nuclear Instruments and Methods in Physics Research Section A: Accel-

480 erators, Spectrometers, Detectors and Associated Equipment 673 (2012)
481 107–110. doi:10.1016/j.nima.2012.01.024.

482 [15] S. F. Biagi, Monte Carlo simulation of electron drift and diffusion
483 in counting gases under the influence of electric and magnetic fields,
484 Nucl. Instrum. Meth. A421 (1-2) (1999) 234–240. doi:10.1016/S0168-
485 9002(98)01233-9.

486 URL <https://magboltz.web.cern.ch/magboltz>



Click here to access/download

LaTeX Source Files (Revised and Final)
elsarticle-template-num.tex

